Research Article

Nano Research
2022, 15(10): 9352–9358

ISSN 1998-0124 CN 11-5974/O4
https://doi.org/10.1007/s12274-022-4564-3

Multimode human–machine interface using a single-channel and patterned triboelectric sensor

Zhiping Feng[1], Qiang He[1], Xue Wang[1], Jing Liu[1], Jing Qiu[1], Yufen Wu[2] (✉), and Jin Yang[1] (✉)

[1] *Department of Optoelectronic Engineering, Key Laboratory of Optoelectronic Technology and Systems Ministry of Education, Chongqing University, Chongqing 400044, China*
[2] *College of Physics and Electronic Engineering, Chongqing Normal University, Chongqing, 401331, China*

Received: 31 March 2022 / **Revised:** 14 May 2022 / **Accepted:** 19 May 2022

ABSTRACT

Triboelectric interfaces have already been extensively researched in the area of human–machine interaction owing to their self-sustainability, low cost, easy manufacturing, and diverse configurations. However, some limitations (e.g., a large number of electrodes, multiple lines, and chunks) observed in previous works hinder the further development of human–machine interaction applications. Herein, a triboelectric encoding interface is proposed by designing the reverse polarity of the tribo-layers to encode the triboelectric output signals. Owing to the inversion of the tribo-layers and the number of strip electrodes, this encoding method can realize multipurpose interactive commands by using fewer electrodes and a simple structure only in one macroscopic triboelectric device, which greatly reduces the size of the device as well as the influence of external factors on the coded signal output. As a demonstration, a ring with the patterned triboelectric interface (15 mm × 20 mm) achieves slide presentation and remote electric device control. In addition, the triboelectric sensor has good sensitivity (1.55 V/N) and durability (> 30,000 cycles). This new encoding mode shows the high applicability of the operation mode in diversified interactive applications, which provides more design strategies for intelligent control.

KEYWORDS

human–machine interfaces, smart control, triboelectric sensor, single electrode, nanostructure

1 Introduction

Human–machine interfaces (HMIs), as bridges of communication between humans and particular devices, are applied in diverse intelligent scenes, such as robotics, input security systems, and smart home and recreational activities using virtual/augmented reality (VR/AR) interfaces, with the aid of advanced technology [1–5]. Remarkable progress has been achieved in HMIs based on various fundamental mechanisms, such as piezoresistive [6–8], piezocapacitive [9, 10], piezoelectric [11–13], and triboelectric effects [14–17]. According to different mechanisms, HMIs can be categorized as non-self-powered and self-powered types, both of which convert external mechanical stimuli into electrical signals. Non-self-powered sensors (piezoresistive and capacitive) benefit from accurate and stable signal acquisition; however, most of them are largely conditional on the development and utilization of novel and modified nanomaterials with new structures [18–21]. In contrast, self-powered sensors with the merits of self-powered capabilities and diversified custom designs, such as triboelectric sensors and piezoelectric sensors, can be applied in more scenarios. On the other hand, to improve the output performance of the sensor, special treatment of the material is required. For example, the piezoelectric effect only exists in specific piezoelectric materials, and the polarization process of piezoelectric materials is indispensable before preparing the device [22]. The complex preparation process inevitably leads to greater energy consumption, which is not in line with the current theme of "carbon neutrality". Therefore, in response to the green and sustainable development path of energy conservation and emission reduction, human–machine interactive equipment with low power consumption, low cost, and high performance needs to be developed.

In recent years, triboelectric nanogenerators (TENGs) have shone in the fields of energy harvesting and self-powered sensing due to the wide selection of materials, cost-effectiveness, structural adaptability, and high electrical output [23–27]. Compared with sensors based on other mechanisms, triboelectric sensors have significant advantages in diversified pattern designs and effective self-powered sensing. Therefore, TENGs can adequately suit the needs of HMIs design because of their ability to generate electricity via almost all types of mechanical motion. The evolution of HMIs with advanced TENG technology has realized a variety of functional interfaces [28–32], which marks the widening of the practicality of interactive equipment and promotes the further development of HMIs. Most HMIs are pressure-sensitive triboelectric sensors, which prompt different instructions according to the presence or absence of signals [28, 33–36]. To develop more multifunctional intelligent HMIs, an array comprising multiple triboelectric pixels is widely adopted. However, more electrodes are required as the sensing pixels increase, which results in large-volume HMIs, complex multi-channel circuits, and heavy signal process [32, 37, 38]. Some studies try to control the amplitude of triboelectric signals by

Address correspondence to Yufen Wu, 20160023@cqnu.edu.cn; Jin Yang, yangjin@cqu.edu.cn

finger bending angle and different pressures to achieve more functions with fewer sensors [39]. However, finger bending angle and pressure are difficult to precisely control, which will cause signal fluctuation. Another optimization scheme is to pattern the triboelectric electrodes to code the triboelectric signals on fewer triboelectric sensors [40–42]. In either case, the large number of sensing electrodes significantly increases the complexity of layout design and device manufacture.

On the basis of the triboelectric device, encoding the voltage output signals from the material polarity is an attractive scheme for further achieving more operation commands with fewer sensors. In this study, a patterned triboelectric sensor designed by inverting tribo-layers is proposed for a multipurpose HMI with a single channel. This combination of material polarity and structural design can help materialize multipurpose interactive commands on a small single-electrode interface. The interface has good merits, including high scalability, robustness and reliability, which is regardless of the variation of sliding force and sliding speed, as the signal detection mechanism is independent of the absolute amplitude. To demonstrate, a ring based on the triboelectric interface was successfully created to control page turning and remotely control an electric device. The advanced information coding concept enables the realization of highly scalable and single-electrode triboelectric interfaces toward diversified applications, including smart control, smart home and smart city.

2 Results and discussion

2.1 The design of the patterned sensor for HMI

To realize multipurpose interactive commands with a single-electrode output, the patterned interface with a new coding method for HMI was introduced. Furthermore, the patterned interface based on the new encoding mode has high scalability with a small sensing area. The patterned interface integrated on a ring indicates that the patterned interface combines merits of being small, flexible, shapeable, and simply constructed (Fig. 1(a)). The layered details of the patterned interface with all the strip electrodes connected into a single-electrode channel are shown, which consist of five stacking thin layers, including a polyethylene terephthalate (PET) substrate (bottom layer), a copper (Cu) electrode, tribo-layer 2, a spacer, tribo-layer 1, and a shielding layer (top layer) (Fig. 1(b)). Two kinds of materials with different orders in the triboelectric series can be selected. To ensure the reliability of results, the thermoplastic polyurethanes (TPU) and polytetrafluoroethylene (PTFE) as internal tribo-layers are applied since PTFE and TPU have significant difference in polarity [43]. By interchanging the two tribo-layers and combining optimal electrodes, the generated output signals with different polarities and peak numbers are used as the coded information. Nanostructures are introduced on the TPU surface by hot-pressing process to improve the sensor output performance. The electron microscope image is shown in Fig. 1(c). The digital photographs of the patterned sensor attached to the ring are shown in Fig. 1(d), where the scale bar is 1 cm. The production details of the sensor are described in Fig. S1 in the Electronic Supplementary Material (ESM). Figures 1(e) and 1(f) exhibit four different finger sliding directions and the corresponding output signals, respectively. As indicated in Fig. 1(e), parts (i) and (ii) are marked as PTFE-TPU(E)s, which represent the tribo-layer 1 (PTFE) and the tribo-layer 2 (TPU) close to the induced electrode. Parts (iii) and (iv) are TPU-PTFE(E)s, indicating that the positions of two tribo-layers are interchanged compared with that of PTFE-TPU(E). The voltage output signals with opposite polarities are produced from the two sensing cells (TPU-PTFE(E) and PTFE-TPU(E)). In this scenario, a negative voltage peak followed by a positive one when sliding across the sensing cell PTFE-TPU(E) is encoded as "0", as shown in Fig. 1(f). A positive voltage peak followed by a negative one from the TPU-PTFE(E) is encoded as "1". When the finger is sliding on the two sensing cells (2 PTFE-TPU(E)s (Fig. 1(e)(ii)), the negative voltage peak followed by a positive one appears twice in the whole motion, which is encoded as "00". Similarly, when sliding across the two TPU-PTFE(E)s, the coding information "11" is obtained due to two completed waveforms (a completed waveform: one positive voltage peak following a negative one). Then, the output peaks with opposing polarity and different numbers can be adopted to encode information on the electrodes, thus realizing multifunctional control for HMIs. It is worth mentioning that the coding method

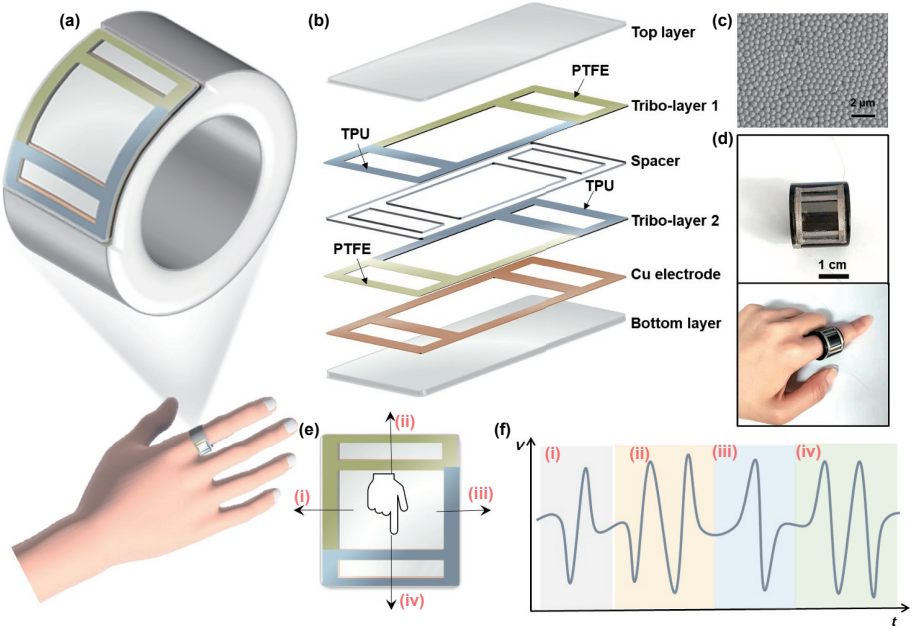

Figure 1 Design configuration and operation principle of the patterned triboelectric sensor. (a) General illustration of the patterned sensor on a ring. (b) Exploded schematic illustration of the sensor. (c) The electron microscopy figure of the TPU nanostructure. (d) Photographs of the patterned sensor attached to the ring and the ring worn on the finger. (e) Four different sliding directions. (f) Output signals corresponding to the four different sliding directions.

related to the polarity of voltage signals but irrelevant to the absolute amplitude can minimize the effects of operation and environment conditions. For example, the absolute amplitude of output voltages may be affected by the applied force, velocity, and device geometry, but the polarity is only determined by the relative orders of tribo-layers in triboelectric serials, which are characteristics of tribo-layers. In addition, the relative polarity of the output signal can be realized by any two tribo-layers with relative orders, thereby proving a wide range of material options.

2.2 Working principle of the patterned sensor

The basic working principle of the interface based on the triboelectric sensor can be explained by adopting the schematics shown in Fig. 2. The basic principle of triboelectric effect is discussed in detail in Fig. S2 in the ESM. The contact–separation mode illustrated in Figs. 2(a) and 2(b) are adopted to expound the contact electrification and electrostatic induction process of PTFE-TPU(E) and TPU-PTFE(E). The induced electrode corresponding to the tribo-layer will expel or attract electrons due to the contact–separation process, thereby generating upward or downward voltage signals in the external circuit. Meanwhile, the number of the generated output peaks is decided by the number of strip electrodes.

2.3 Optimization of sensor performance

As a basic pressure sensor, the pressure perception ability is an essential element, which is characterized by sensitivity—a crucial parameter of the output performance. Here, the sensitivity is defined as $S = \Delta V/\Delta F$, where ΔV is the change in the output voltage and ΔF is the change in the external pressure. The self-built test platform is shown in Fig. S4 in the ESM. An electrical output of a 10 mm × 10 mm sensor was characterized for pressure sensing when a wide range of pressures (0–5 N) with a frequency of 5 Hz was applied to the sensor, as shown in Fig. 3(a). The obtained sensitivity has two stages in the applied pressure ranges. When the external pressure is less than 4 N, the sensitivity is 1.55 V/N, whereas a sensitivity of 0.11 V/N is acquired in the high-pressure region (4–10 N). This phenomenon is due to the difference in the contact–separate area of two tribo-layers under different external pressures, and the effective contact separation area no longer changes significantly when the pressure reaches a certain critical value [44, 45]. The inset indicates that the output voltages of the sensor are in the range of 1–5 N, and clearly distinct voltage outputs can be observed. Meanwhile, the durable mechanical property of the sensor is also critical for long-term practice, so the stability of the sensor was investigated with a stable force of 3 N and a fixed frequency of 10 Hz applied. Data with a total of 30,000 loading–unloading cycles were recorded, and the open-circuit voltage of the sensor is depicted in Fig. 3(b), showing that the sensor enjoys good durability. Because the tribo-charges on the human body or other touching objects may influence the amplitude or polarity of the voltage output signal, the shield film for maintaining the intrinsic characteristics of the voltage output signal in the sensor is essential [46]. As shown in Figs. 3(c) and 3(d), the polarity of the voltage output signal may change if the sensor is without a shield film. Due to the shield film, the intrinsic polarity of the voltage output signal can be protected to be consistent with the mechanism of electrostatic induction. Figure 3(e) illustrates the influence of electrode width on the output performance of the sensor; the measurements were conducted with electrode width varying between 8, 6, 4, and 2 mm. With the increase in electrode width, the amplitude of signal output becomes larger at the same applied force (0.5 N, 1 Hz) because of the increased contact area between the two tribo-layers. Moreover, the signal output amplitudes of PTFE(E)-TPU and PTFE-TPU(E) have a consistent increased variation trend as the electrode width increases, proving that the sensor has effective signal output in the selected range of electrode width. Finding a suitable interval between two strip electrodes is essential to distinguish the number of peaks. To find the optimal electrode spacing distance, the effects of greater electrode spacings (6, 5, 4, 3, 2, and 1 mm) on the output signal peaks were explored. As shown in Fig. 3(f), the results indicate that two clear separated output peaks are observed, even at the 1 mm interval, which contributes to the possibility of device miniaturization.

2.4 The characterization of the patterned triboelectric interface

The patterned triboelectric interface was investigated in terms of output signal generation under different sliding pressures and speeds. As shown in Figs. 4(a) and 4(b), the amplitudes of voltage output corresponding to the four directions increase with the sliding pressure varying from low to high (0.5, 1 and 2 N) at a relatively constant speed. Next, the characterizations were

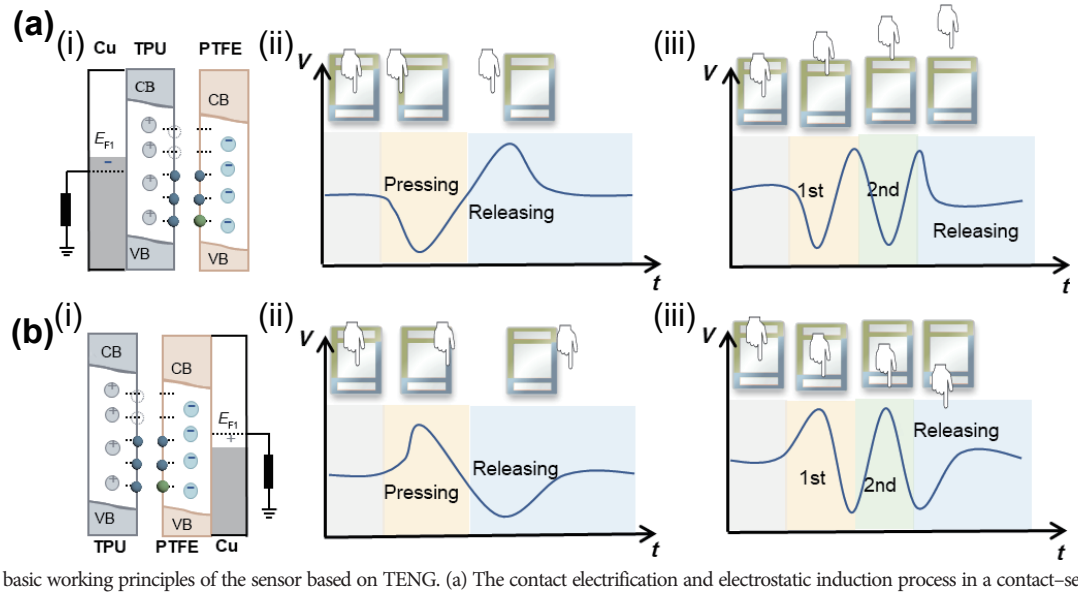

Figure 2 The basic working principles of the sensor based on TENG. (a) The contact electrification and electrostatic induction process in a contact–separation mode and detailed working principle of PTFE-TPU(E). (b) The contact electrification and electrostatic induction process in a contact–separation mode and detailed working principle of PTFE(E)-TPU.

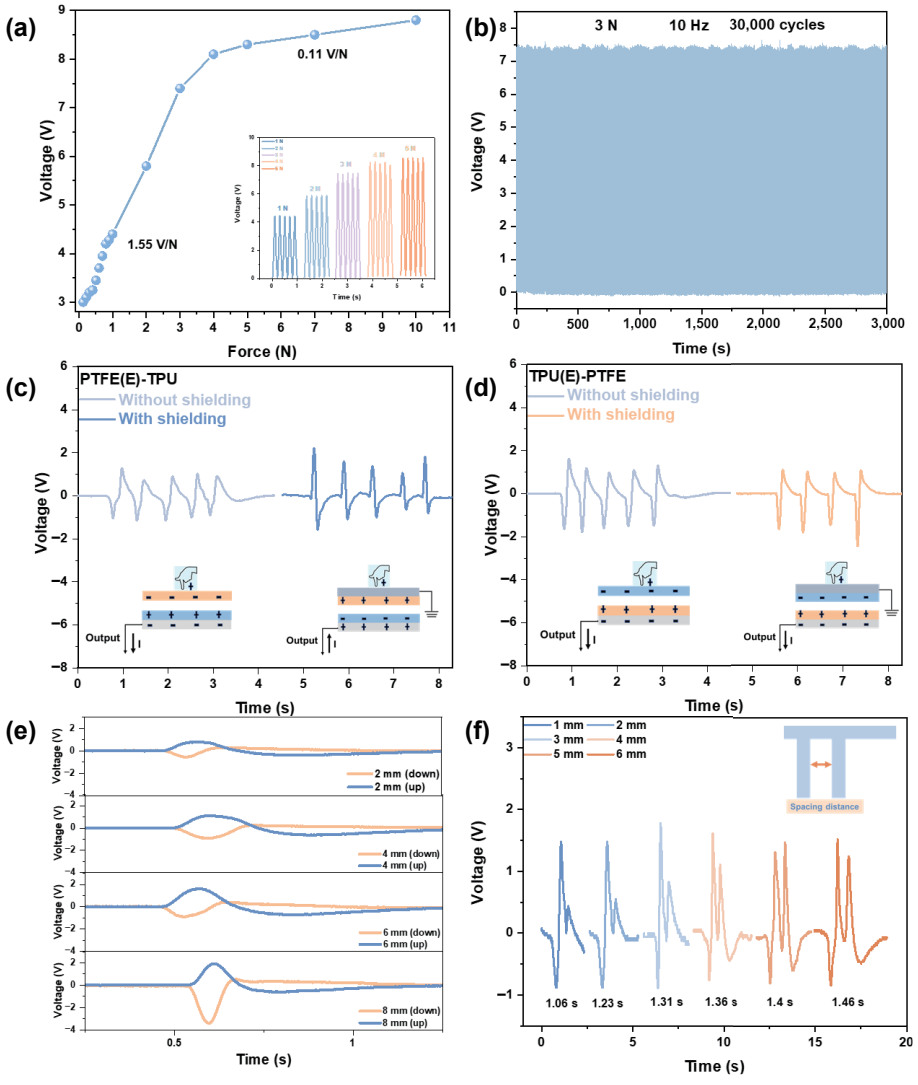

Figure 3 The sensor performance and optimization. (a) The electrical characterization of the sensor in response to pressure. (b) The mechanical durability characterization of the sensor under an applied force (3 N, 10 Hz) for 30,000 cycles. The effect of shield film on (c) PTFE(E)-TPU and (d) PTFE-TPU(E). (e) The effect of electrode width on the sensor performance. (f) The spacing distance of sensor electrodes influencing the output performance of the sensor.

performed to investigate the voltage output signals varying with the sliding speed. The speed is determined by the time spent at a fixed distance, i.e., slow (4.16–5.50 mm/s), normal (8.10–9.67 mm/s) and fast (14.28–15.78 mm/s). The voltage output peaks from the four directions (insets showing sliding directions) can be clearly identified for three different finger sliding speeds increasing from slow to fast, as shown in Figs. 4(c) and 4(d). It is worth mentioning that the variation of the sliding force and speed will not change the polarity of the signal output, which once again shows the reliability of the encoded polarity signal.

2.5 Application of the patterned triboelectric interface

As proof of the concept, we demonstrated the applications of smart rings for controlling slides and lamps, as shown in Fig. 4. The block diagram of the control system is depicted in Fig. 5(a), which presents the data flow of signal reception and processing, including the smart ring, signal acquisition and processing circuit, signal identification, and the displays of the controlling application. After the output signal is generated from the smart ring when the thumb slips across from the interface, the signal is received and processed by the functional circuit. A photograph of functional circuit is shown in Fig. S5 in the ESM. Subsequently, the filtered and amplified signal is detected and identified by the computer. According to the identified signal, the slides and lights are controlled to perform actions in accordance with the instructions. The insets in Fig. 5(b) depict the four directions of sliding from the patterned interface. The corresponding voltage pulse waveforms emerge to achieve different control commands for the controlling slide, such as slide presentation, stop presentation, last slide, and next slide, as shown in Fig. 5(b). The positive or negative charges of the voltage output peaks only depend on the position of the two tribo-layers relative to the inducted electrode, which is undisturbed by the external force. This could change the polarity of the voltage output signal, thereby ensuring the accuracy of the recognition of the instructions based on the interface. The accuracy of control commands based on the patterned interface is demonstrated in Fig. 5(c). In 100 experiments with the finger sliding under random speeds across the interface, the accuracy for the four encoding modes is around 90%, where the encoding modes of "0" and "1" are above 90% and the encoding modes of "00" and "11" are below 90%. The stable low-speed sliding accuracy is shown in Fig. S6 in the ESM, where all accuracies are above 95%. The superior accuracy further ensures the accurate control command of the interface. In Fig. 5(d)(i) and Video ESM1, the slideshow controlled by the smart ring is successfully demonstrated. The wearable device with a new encoding method introduced to manipulate the slides is more convenient as opposed to using a laser pointer, indicating the stylish portability of the new encoding device and an unconstrained operation. The second demonstration of

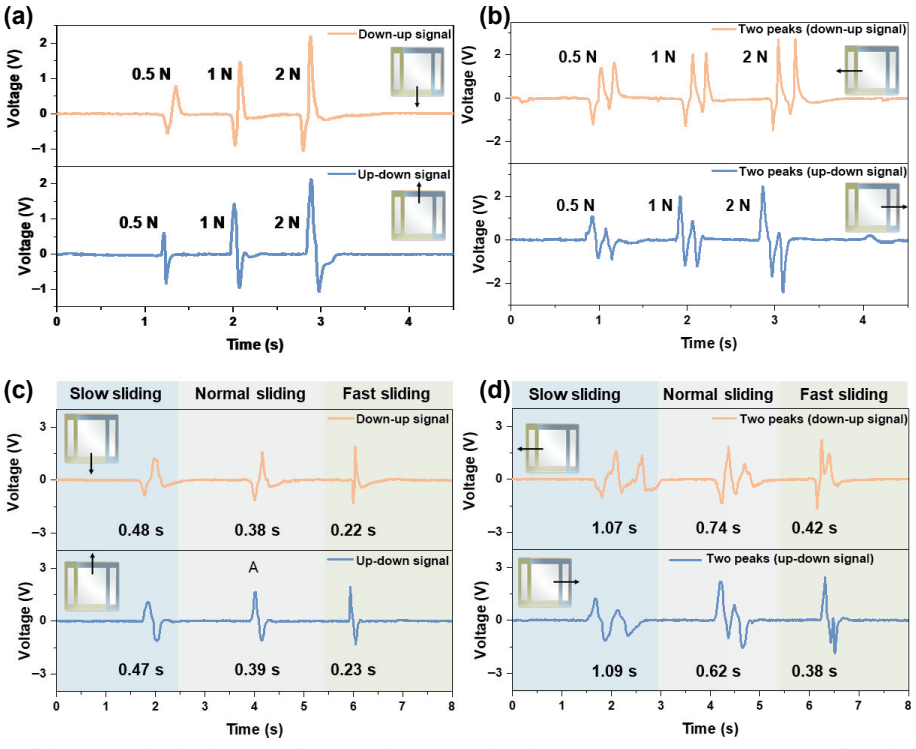

Figure 4 Characterization of the patterned triboelectric interface. (a) The single-peak and (b) two-peak voltage output signals from the interface under different sliding forces (0.5, 1 and 2 N). (c) The generated single-peak and (d) two-peak voltage output signals from the interface with slow, normal, and fast sliding speeds.

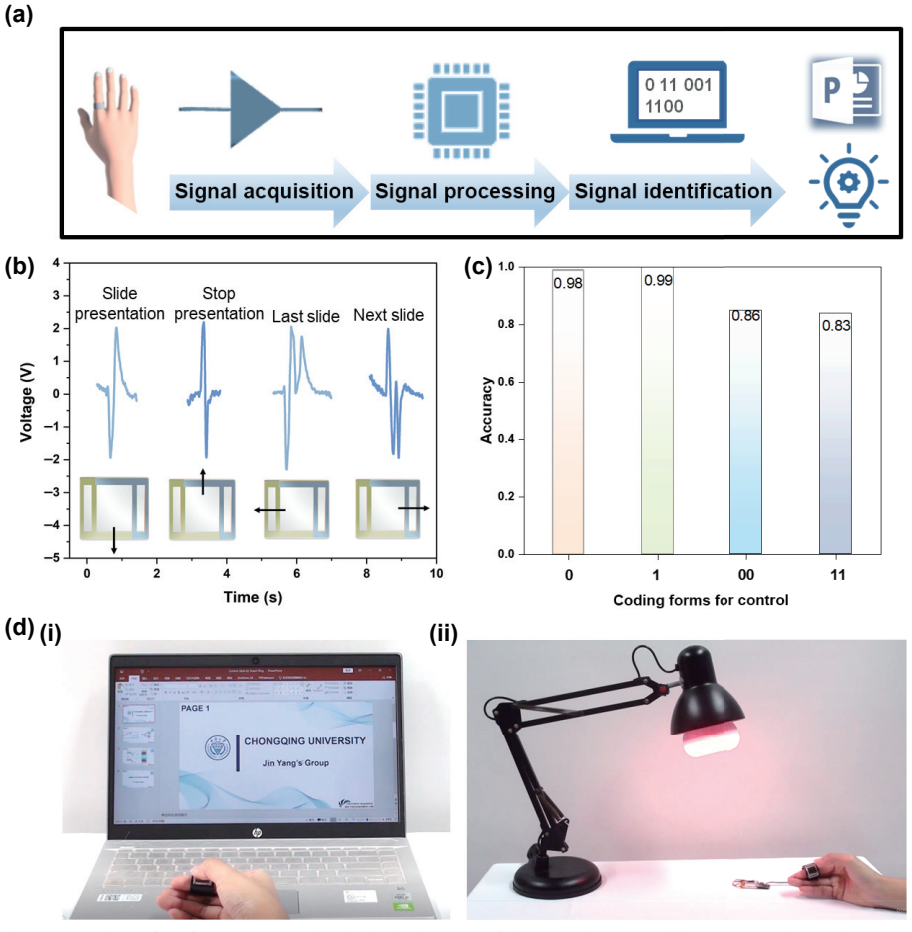

Figure 5 Application of the patterned interface for HMI control. (a) Block diagram of the control system. (b) Corresponding voltage output signals of the control commands. (c) Accuracy of each command for the slideshow. (d) Screenshot of the video demonstration.

controlling lamps in modern smart room is shown in Fig. 5(d)(ii) and Video ESM2. When the finger Is drawn across the four areas on the smart ring, the light could be turned on and off, as well as the brightness could be successfully adjusted. In addition, the patterned triboelectric interface has more scalable encoding forms. For example, defining more encoding forms by sliding in two directions within a fixed time can be extended to six encoding forms, as shown in Fig. S7 in the ESM. Therefore, adopting the

signal polarity instead of signal amplitude as encoded information provides the new coding strategy, which provides an economical, portable, unconstrained, and wearable interface for HMI application scenarios.

3 Conclusion

In summary, the patterned HMI based on the triboelectric sensor with the new encoding mode was developed to successfully achieve multipurpose control commands. The encoding design was carried out according to the polarity of the voltage signal, not the absolute amplitude to immunize against the influence of environment and human operation. By adopting different numbers of strip electrodes, the expansion space is greatly reduced due to the single-electrode output. Compared with the previously reported triboelectric coding mode, this new coding method exhibits superior advantages of high scalability, conciseness, and reliability in various usage scenarios. In addition, controlling slideshow and lamp using the patterned interface attached to a ring is successfully demonstrated. Moreover, a 10 mm × 10 mm triboelectric sensor has compelling comprehensive properties, where the sensitivity is high to 1.55 V/N and the stability lasts more than 30,000 cycles—a decent value. This new encoding strategy provides great potential in various usage scenarios, including two-dimensional (2D)/three-dimensional (3D) control, VR/AR, wearable electronics, robotics, smart home, and internet of things (IoT).

4 Methods

4.1 Fabrication of the triboelectric interface

Materials: All materials were purchased online and used directly without further processing.

Fabrication of TPU rough surface: The rough nano-surface was obtained by pressing melting TPU onto the surface of anodic aluminium oxide (AAO) template at a high temperature (120 °C), Then the TPU was cooled to room temperature and the AAO template was etched in chemical solutions. Afterwards, the obtained TPU rough surface was further washed with distilled water and dried at 60 °C for 1 h.

Fabrication of the interface: First, the copper tape electrode was cut into a suitable size (2 mm width) and all electrodes were connected together to form a patterned electrode with a single channel. The minimum interval between two electrodes was 2 mm, and the maximum interval was more than 10 mm. Next the patterned electrode was divided into two parts and TPU and PTFE (the size corresponding to the electrode) were pasted as the first tribo-layers on the electrodes, respectively. PET (thickness of 0.2 mm) was as the edge spacer. Then another tribo-layer (PTFE and TPU) was pasted opposite to the first tribo-layers (TPU and PTFE) to form the sensing cells-PTFE(E)-TPU and TPU(E)-PTFE respectively. Finally, the shielding film was cited to avoid external interference. A cost-effective and patterned interface with a size of 15 mm × 20 mm was successfully manufactured.

4.2 Characterization of the interface

The output voltage of the interface was measured by a DSO-X3034A oscilloscope (Tektronix) with a high impedance probe of 100 MΩ. The repeatable experiment was tested by a self-built platform, in which the visual signal output and storage were realized by a Labview host computer.

Acknowledgements

This work was supported by the National Natural Science Foundation of China (No. 51675069 and 51775070), the Natural Science Foundation of Innovative Research Groups (No cstc2020jcyj-cxttX0005), the Fundamental Research Funds for the Central Universities (Nos. 2018CDQYGD0020 and cqu2018CDHB1A05), the Scientific And Technological Research Program Of Chongqing Municipal Education Commission (No. KJ1703047), and the Natural Science Foundation Projects of Chongqing(Nos. cstc2017shmsA40018 and cstc2018jcyjAX0076).

Electronic Supplementary Material: Supplementary material (the AAO removing process; fabrication process of the patterned sensor (Fig. S1); the basic principle of TENG sensor (Fig. S2); the change of the electric potential as the increasement of distance simulated by COMSOL software (Fig. S3); a self-designed testing system (Fig. S4); a photograph of the functional circuit (Fig. S5); the accuracy of encoding mode in stable slow mode (Fig. S6); extensible encoding forms (Fig. S7). Video ESM1: Control slideshows remotely by the patterned interface attached to the ring (MP4); Video ESM2: Control lights on, off and adjust brightness by the patterned HMI interface (MP4)) is available in the online version of this article at https://doi.org/10.1007/s12274-022-4564-3.

References

[1] Huang, Y.; Fan, X. Y.; Chen, S. C.; Zhao, N. Emerging technologies of flexible pressure sensors: Materials, modeling, devices, and manufacturing. *Adv. Funct. Mater.* **2019**, *29*, 1808509.

[2] Wang, X. D.; Dong, L.; Zhang, H. L.; Yu, R. M.; Pan, C. F.; Wang, Z. L. Recent progress in electronic skin. *Adv. Sci. (Weinh.)* **2015**, *2*, 1500169.

[3] Singh, H. P.; Kumar, P. Developments in the human machine interface technologies and their applications: A review. *J. Med. Eng. Technol.* **2021**, *45*, 552–573.

[4] Heng, W. Z.; Solomon, S.; Gao, W. Flexible electronics and devices as human–machine interfaces for medical robotics. *Adv. Mater.* **2022**, *34*, 2107902.

[5] Zhao, X.; Askari, H.; Chen, J. Nanogenerators for smart cities in the era of 5G and internet of things. *Joule* **2021**, *5*, 1391–1431.

[6] Esposito, D.; Andreozzi, E.; Gargiulo, G. D.; Fratini, A.; D'Addio, G.; Naik, G. R.; Bifulco, P. A piezoresistive array armband with reduced number of sensors for hand gesture recognition. *Front. Neurorobot.* **2019**, *13*, 114.

[7] Wang, J.; Xu, J. M.; Chen, T.; Song, L. L.; Zhang, Y. L.; Lin, Q. H.; Wang, M. J.; Wang, F. X.; Ma, N. H.; Sun, L. N. Wearable human–machine interface based on the self-healing strain sensors array for control interface of unmanned aerial vehicle. *Sens. Actuat. A:Phys.* **2021**, *321*, 112583.

[8] Zhang, H. J.; Han, W. Q.; Xu, K.; Zhang, Y.; Lu, Y. F.; Nie, Z. T.; Du, Y. H.; Zhu, J. X.; Huang, W. Metallic sandwiched-aerogel hybrids enabling flexible and stretchable intelligent sensor. *Nano Lett.* **2020**, *20*, 3449–3458.

[9] Zhao, S. F.; Ran, W. H.; Wang, D. P.; Yin, R. Y.; Yan, Y. X.; Jiang, K.; Lou, Z.; Shen, G. Z. 3D dielectric layer enabled highly sensitive capacitive pressure sensors for wearable electronics. *ACS Appl. Mater. Interfaces* **2020**, *12*, 32023–32030.

[10] Zulfiqar, M. H.; Hassan, M. U.; Zubair, M.; Mehmood, M. Q.; Riaz, K. Pencil-on-paper-based touchpad for ecofriendly and reusable human–machine interface. *IEEE Sens. Lett.* **2021**, *5*, 5500604.

[11] Deng, W. L.; Yang, T.; Jin, L.; Yan, C.; Huang, H. C.; Chu, X.; Wang, Z. X.; Xiong, D.; Tian, G.; Gao, Y. Y. et al. Cowpea-structured PVDF/ZnO nanofibers based flexible self-powered piezoelectric bending motion sensor towards remote control of gestures. *Nano Energy* **2019**, *55*, 516–525.

[12] Gong, S. B.; Zhang, B. W.; Zhang, J. X.; Wang, Z. L.; Ren, K. L. Biocompatible poly(lactic acid)-based hybrid piezoelectric and electret nanogenerator for electronic skin applications. *Adv. Funct. Mater.* **2020**, *30*, 1908724.

[13] Wang, H. S.; Hong, S. K.; Han, J. H.; Jung, Y. H.; Jeong, H. K.; Im,

T. H.; Jeong, C. K.; Lee, B. Y.; Kim, G.; Yoo, C. D. et al. Biomimetic and flexible piezoelectric mobile acoustic sensors with multiresonant ultrathin structures for machine learning biometrics. *Sci. Adv.* **2021**, *7*, eabe5683.

[14] He, Q.; Wu, Y. F.; Feng, Z. P.; Sun, C. C.; Fan, W. J.; Zhou, Z. H.; Meng, K. Y.; Fan, E. D.; Yang, J. Triboelectric vibration sensor for a human–machine interface built on ubiquitous surfaces. *Nano Energy* **2019**, *59*, 689–696.

[15] Zhou, Z. H.; Chen, K.; Li, X. S.; Zhang, S. L.; Wu, Y. F.; Zhou, Y. H.; Meng, K. Y.; Sun, C. C.; He, Q.; Fan, W. J. et al. Sign-to-speech translation using machine-learning-assisted stretchable sensor arrays. *Nat. Electron.* **2020**, *3*, 571–578.

[16] Dong, B. W.; Shi, Q. F.; Yang, Y. Q.; Wen, F.; Zhang, Z. X.; Lee, C. Technology evolution from self-powered sensors to AIoT enabled smart homes. *Nano Energy* **2021**, *79*, 105414.

[17] Libanori, A.; Chen, G. R.; Zhao, X.; Zhou, Y. H.; Chen, J. Smart textiles for personalized healthcare. *Nat. Electron.* **2022**, *5*, 142–156.

[18] Ding, X. C.; Zhong, W. B.; Jiang, H. Q.; Li, M. F.; Chen, Y. L.; Lu, Y.; Ma, J.; Yadav, A.; Yang, L. Y.; Wang, D. Highly accurate wearable piezoresistive sensors without tension disturbance based on weaved conductive yarn. *ACS Appl. Mater. Interfaces* **2020**, *12*, 35638–35646.

[19] Cao, M. H.; Fan, S. Q.; Qiu, H. W.; Su, D. L.; Li, L.; Su, J. CB nanoparticles optimized 3D wearable graphene multifunctional piezoresistive sensor framed by loofah sponge. *ACS Appl. Mater. Interfaces* **2020**, *12*, 36540–36547.

[20] Mishra, R. B.; El-Atab, N.; Hussain, A. M.; Hussain, M. M. Recent progress on flexible capacitive pressure sensors: From design and materials to applications. *Adv. Mater. Technol.* **2021**, *6*, 2001023.

[21] Jiang, P. P.; Qin, H. L.; Dai, J.; Yu, S. H.; Cong, H. P. Ultrastretchable and self-healing conductors with double dynamic network for omni-healable capacitive strain sensors. *Nano Lett.* **2022**, *22*, 1433–1442.

[22] Mahapatra, S. D.; Mohapatra, P. C.; Aria, A. I.; Christie, G.; Mishra, Y. K.; Hofmann, S.; Thakur, V. K. Piezoelectric materials for energy harvesting and sensing applications: Roadmap for future smart materials. *Adv. Sci. (Weinh.)* **2021**, *8*, 2100864.

[23] Fan, F. R.; Tian, Z. Q.; Wang, Z. L. Flexible triboelectric generator. *Nano Energy* **2012**, *1*, 328–334.

[24] Kim, W. G.; Kim, D. W.; Tcho, I. W.; Kim, J. K.; Kim, M. S.; Choi, Y. K. Triboelectric nanogenerator: Structure, mechanism, and applications. *ACS Nano* **2021**, *15*, 258–287.

[25] Chen, C. Y.; Chen, L. J.; Wu, Z. Y.; Guo, H. Y.; Yu, W. D.; Du, Z. Q.; Wang, Z. L. 3D double-faced interlock fabric triboelectric nanogenerator for bio-motion energy harvesting and as self-powered stretching and 3D tactile sensors. *Mater. Today* **2020**, *32*, 84–93.

[26] Chen, G. R.; Xiao, X.; Zhao, X.; Tat, T.; Bick, M.; Chen, J. Electronic textiles for wearable point-of-care systems. *Chem. Rev.* **2022**, *122*, 3259–3291.

[27] Zhang, S. L.; Bick, M.; Xiao, X.; Chen, G. R.; Nashalian, A.; Chen, J. Leveraging triboelectric nanogenerators for bioengineering. *Matter* **2021**, *4*, 845–887.

[28] Chen, J. L.; Wen, X. J.; Liu, X.; Cao, J. Q.; Ding, Z. H.; Du, Z. Q. Flexible hierarchical helical yarn with broad strain range for self-powered motion signal monitoring and human–machine interactive. *Nano Energy* **2021**, *80*, 105446.

[29] Gao, L. X.; Hu, D. L.; Qi, M. K.; Gong, J.; Zhou, H.; Chen, X.; Chen, J. F.; Cai, J.; Wu, L. K.; Hu, N. et al. A double-helix-structured triboelectric nanogenerator enhanced with positive charge traps for self-powered temperature sensing and smart-home control systems. *Nanoscale* **2018**, *10*, 19781–19790.

[30] Ding, W. B.; Wang, A. C.; Wu, C. S.; Guo, H. Y.; Wang, Z. L. Human–machine interfacing enabled by triboelectric nanogenerators and tribotronics. *Adv. Mater. Technol.* **2019**, *4*, 1800487.

[31] Hou, C.; Geng, J. J.; Yang, Z.; Tang, T. Y.; Sun, Y. Y.; Wang, F. X.; Liu, H. C.; Chen, T.; Sun, L. N. A delta-parallel-inspired human machine interface by using self-powered triboelectric nanogenerator toward 3D and VR/AR manipulations. *Adv. Mater. Technol.* **2021**, *6*, 2000912.

[32] Yun, J.; Jayababu, N.; Kim, D. Self-powered transparent and flexible touchpad based on triboelectricity towards artificial intelligence. *Nano Energy* **2020**, *78*, 105325.

[33] Zhao, G. Q.; Yang, J.; Chen, J.; Zhu, G.; Jiang, Z. D.; Liu, X. Y.; Niu, G. X.; Wang, Z. L.; Zhang, B. Keystroke dynamics identification based on triboelectric nanogenerator for intelligent keyboard using deep learning method. *Adv. Mater. Technol.* **2019**, *4*, 1800167.

[34] Jeon, S. B.; Park, S. J.; Kim, W. G.; Tcho, I. W.; Jin, I. K.; Han, J. K.; Kim, D.; Choi, Y. K. Self-powered wearable keyboard with fabric based triboelectric nanogenerator. *Nano Energy* **2018**, *53*, 596–603.

[35] Zhang, B. S.; Tang, Y. J.; Dai, R. R.; Wang, H. Y.; Sun, X. P.; Qin, C.; Pan, Z. F.; Liang, E. J.; Mao, Y. C. Breath-based human–machine interaction system using triboelectric nanogenerator. *Nano Energy* **2019**, *64*, 103953.

[36] Rana, S. M. S.; Rahman, M. T.; Salauddin, M.; Sharma, S.; Maharjan, P.; Bhatta, T.; Cho, H.; Park, C.; Park, J. Y. Electrospun PVDF-TrFE/MXene nanofiber mat-Based triboelectric nanogenerator for smart home appliances. *ACS Appl. Mater. Interfaces* **2021**, *13*, 4955–4967.

[37] Pu, X. J.; Tang, Q.; Chen, W. S.; Huang, Z. Y.; Liu, G. L.; Zeng, Q. X.; Chen, J.; Guo, H. Y.; Xin, L. M.; Hu, C. G. Flexible triboelectric 3D touch pad with unit subdivision structure for effective XY positioning and pressure sensing. *Nano Energy* **2020**, *76*, 105047.

[38] Sun, J. L.; Chang, Y.; Dong, L.; Zhang, K. K.; Hua, Q. L.; Zang, J. H.; Chen, Q. S.; Shang, Y. Y.; Pan, C. F.; Shan, C. X. MXene enhanced self-powered alternating current electroluminescence devices for patterned flexible displays. *Nano Energy* **2021**, *86*, 106077.

[39] Pu, X. J.; Guo, H. Y.; Tang, Q.; Chen, J.; Feng, L.; Liu, G. L.; Wang, X.; Xi, Y.; Hu, C. G.; Wang, Z. L. Rotation sensing and gesture control of a robot joint via triboelectric quantization sensor. *Nano Energy* **2018**, *54*, 453–460.

[40] Shi, Q. F.; Lee, C. Self-powered bio-inspired spider-net-coding interface using single-electrode triboelectric nanogenerator. *Adv. Sci. (Weinh.)* **2019**, *6*, 1900617.

[41] Shi, Q. F.; Zhang, Z. X.; Chen, T.; Lee, C. Minimalist and multi-functional human machine interface (HMI) using a flexible wearable triboelectric patch. *Nano Energy* **2019**, *62*, 355–366.

[42] Shi, Q. F.; Qiu, C. K.; He, T. Y. Y.; Wu, F.; Zhu, M. L.; Dziuban, J. A.; Walczak, R.; Yuce, M. R.; Lee, C. Triboelectric single-electrode-output control interface using patterned grid electrode. *Nano Energy* **2019**, *60*, 545–556.

[43] Yoon, H. J.; Ryu, H.; Kim, S. W. Sustainable powering triboelectric nanogenerators: Approaches and the path towards efficient use. *Nano Energy* **2018**, *51*, 270–285.

[44] Liao, W. Q.; Liu, X. K.; Li, Y. Q.; Xu, X.; Jiang, J.; Lu, S. R.; Bao, D. Q.; Wen, Z.; Sun, X. H. Transparent, stretchable, temperature-stable and self-healing ionogel-based triboelectric nanogenerator for biomechanical energy collection. *Nano Res.* **2022**, *15*, 2060–2068.

[45] Bai, Z. Q.; He, T. Y. Y.; Zhang, Z. X.; Xu, Y. L.; Zhang, Z. X.; Shi, Q. F.; Yang, Y. Q.; Zhou, B. G.; Zhu, M. L.; Guo, J. S. et al. Constructing highly tribopositive elastic yarn through interfacial design and assembly for efficient energy harvesting and human-interactive sensing. *Nano Energy* **2022**, *94*, 106956–106968.

[46] Ren, Z. W.; Nie, J. H.; Shao, J. J.; Lai, Q. S.; Wang, L. F.; Chen, J.; Chen, X. Y.; Wang, Z. L. Fully elastic and metal-free tactile sensors for detecting both normal and tangential forces based on triboelectric nanogenerators. *Adv. Funct. Mater.* **2018**, *28*, 1802989.